Supplemental Material for

Quick Identification of ABC Trilayer Graphene at Nanoscale Resolution via a Near-field Optical Route

Peiyue Shen[1,2], Xianliang Zhou[1,2], Jiajun Chen[1,2], Aolin Deng[1,2], Bosai Lyu[1,2], Zhichun Zhang[1,2], Shuo Lou[1,2], Saiqun Ma[1,2], Binbin Wei[3], Zhiwen Shi[1,2*]

[1]Key Laboratory of Artificial Structures and Quantum Control (Ministry of Education), Shenyang National Laboratory for Materials Science, School of Physics and Astronomy, Shanghai Jiao Tong University, Shanghai 200240, China.

[2]Collaborative Innovation Center of Advanced Microstructures, Nanjing University, Nanjing 210093, China.

[3]Institute of System Engineering, Beijing 100191, China

*Correspondence to: zwshi@sjtu.edu.cn

Section I. Preparatory works for selecting samples.

Before the near-field IR measurements, we preliminarily use an optical microscope (Fig. S1a) to estimate the layer number of graphene samples by optical contrast. Then we use scanning near-field optical microscopy (SNOM) with a CO_2 laser (~10.6 μm) to select samples with good domain shapes (Fig. S1b). After that, we use the half widths (HWs) of the Raman 2D peak to confirm layer number as well as stacking order with a homemade Raman spectroscopy system as Fig. S2a shows. The HWs got in our experiment were slightly bigger than those in the previous report[1]. A pair of a typical trilayer's 2D peak data is shown in Fig. S2b, where the ABC trilayer has a small red shift as well as wider HW[2].

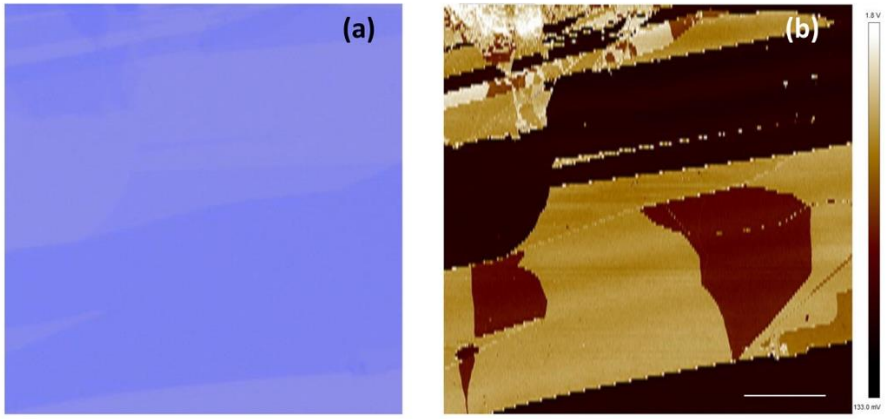

Figure S1. The methods for roughly selecting trilayer samples with suitable domains by optical microscopy **(a)** and SNOM with a CO_2 laser (~10.6 μm) **(b)**. Scale bar: 10 μm.

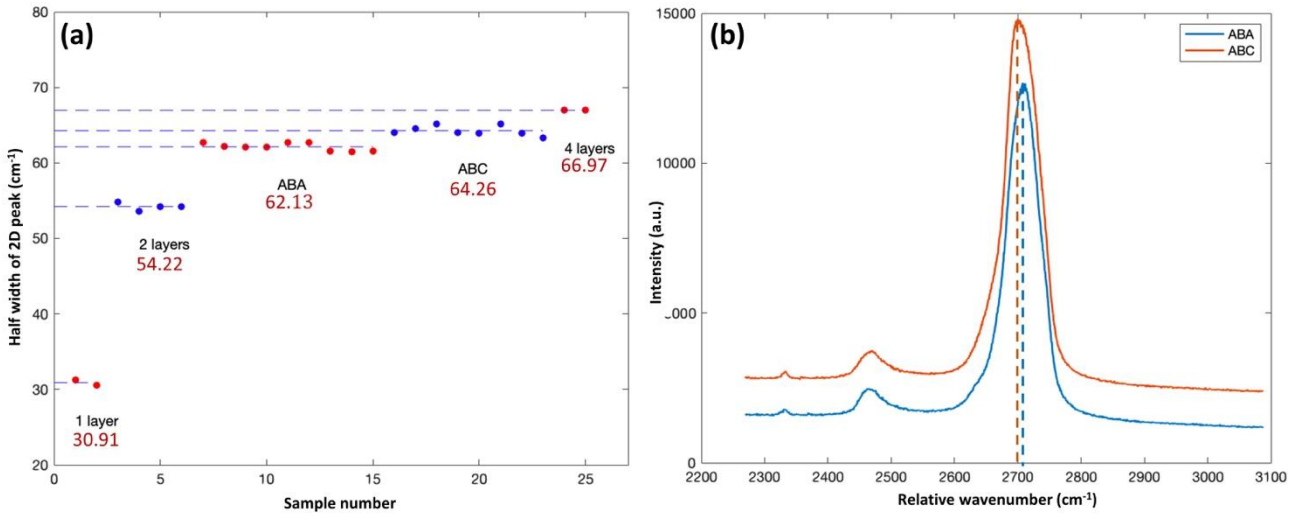

Figure S2. Raman spectra for confirming layer number and stacking order of samples before formal SNOM measurements. (a) The HWs of 2D peaks in the Raman spectra. The red numbers are the average HWs in wave

number unit cm^{-1} for 1~4 layers of graphene. **(b)** A group of representative 2D Raman peaks of ABA and ABC, where ABC is more asymmetry with wider peak half width and a small red-shift of peak position.

Section II. Key Fano parameters for more trilayer samples.

The Fano parameters extracted from data are slightly different among different samples, as Table. S1 show. Especially, sample 1 has a larger linewidth than other samples exhibited, perhaps due to the much greater strain in this sample.

Table S1. Key Fano parameters for different trilayer samples.

Number	V_g/V	q	γ/cm^{-1}	HW	E_0/cm^{-1}	E_{max}/cm^{-1}
Sample in Fig.2	+80	6.1	1.2	2.5	1582.9	1583.1
	+40	7.0	2.4	5.0	1582.3	1582.6
Sample1	-80	6.4	6.3	13.2	1577.1	1578.1
	-60	3.6	6.2	14.5	1578.5	1580.2
Sample2	+60	7.6	1.3	2.7	1584.0	1584.2
Sample3	-60	2.4	4.5	12.8	1581.3	1583.2
Sample4	-40	3.9	3.2	7.3	1582.8	1583.6

Here factors q, γ, and E_0 are parameters extracted by fitting data with the Fano formula[3]

$$A(E) = A_0 \frac{[q\gamma + E - E_0]^2}{(E-E_0)^2 + \gamma^2} ,$$

HW is for the half-width of Fano peaks calculated by $HW = 2\gamma \frac{q^2+1}{q^2-1}$, and E_{max} is the position of Fano peak summits.

Section III. Additional data for gate dependence of trilayer graphene.

Figure S3 shows the possible mechanism for the suppressed SNOM signal of ABA at high gate voltage. When the Fermi level E_F is at the Dirac point (Fig. S3a), the electron transitions make contributions to ABA's near-field signal. When E_F is pulled away by high bias, some electron transitions are blocked due to the Pauli principle (Fig. S3b), thus perhaps leading to the suppression of ABA's near-field signal.

Figure S4 shows other sets of trilayer's signal varying with bias, where ABC is enhanced under high effective voltage while ABA is suppressed, showing the same tendency as the main text exhibits, confirming that the decay of ABA's signal at high voltage is not an accident.

Figure S5 shows a trilayer piece with a high ratio ABC/ABA~2.91 at 1583 cm^{-1} with V_g= +80V, a good contrast between different stacking orders at the resonance frequency.

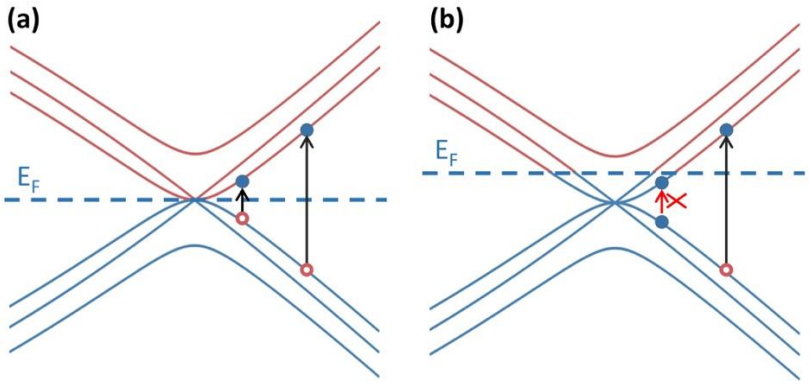

Figure S3. The diagrams of the possible mechanism for the suppressed signal of ABA at the higher voltage in Fig. 3. (a) The electron transitions when Fermi level E_F is at the Dirac point. **(b)** When the Fermi level is lifted with gate V_g increasing, some electron transitions are blocked due to the Pauli principle.

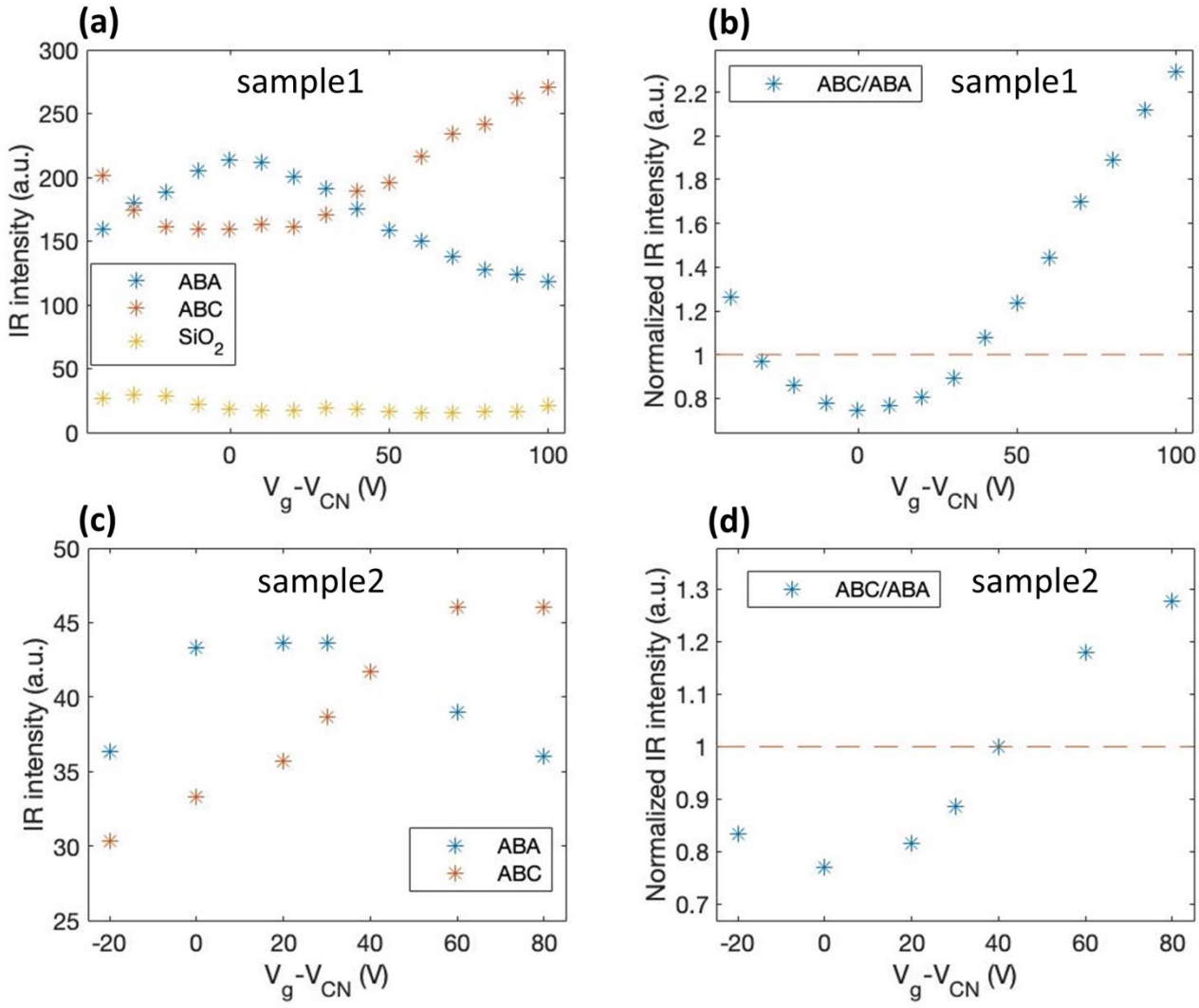

Figure S4. Other groups of trilayer signals against gate voltage at 1585 cm^{-1}. (a) The primary data of both ABC

and ABA trilayers and the background SiO_2 as the reference. ABC and ABA show the same tendency as Fig. 3 in the main text. **(b)** The ratio ABC/ABA. **(c-d)** Similar data for another sample.

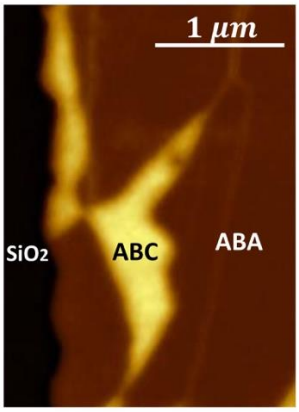

Figure S5. A trilayer piece with a high ratio ABC/ABA at 1583 cm^{-1} with V_g= +80V. The near-field IR signals for ABA and ABC are 0.308 (a.u.) and 0.895 (a.u.), respectively. The ratio of ABC to ABA is about 2.91, a significant contrast.

Section IV. ABA trilayer's behaviors against both voltage and frequency.

Figure S6 displays the horizontal and vertical linecuts of Fig. 4a to better present ABA's behaviors, both of which show that the ABA trilayer behaves much more inertly than the ABC trilayer against both electric bias and excitation frequency. In Fig. S6a, within the whole frequency range, the ABA signal's gate dependence almost keeps the same line shape with intensity becoming slightly weaker when the Fermi level goes far away from the Dirac point. In Fig. S6b, under different voltages, the ABA trilayer behaves as almost a constant against excitation frequency, with only a tiny peak that can be observed around the phonon frequency. But the intensity of that Fano peak is much smaller than the ABC's, in agreement with the previous report[4].

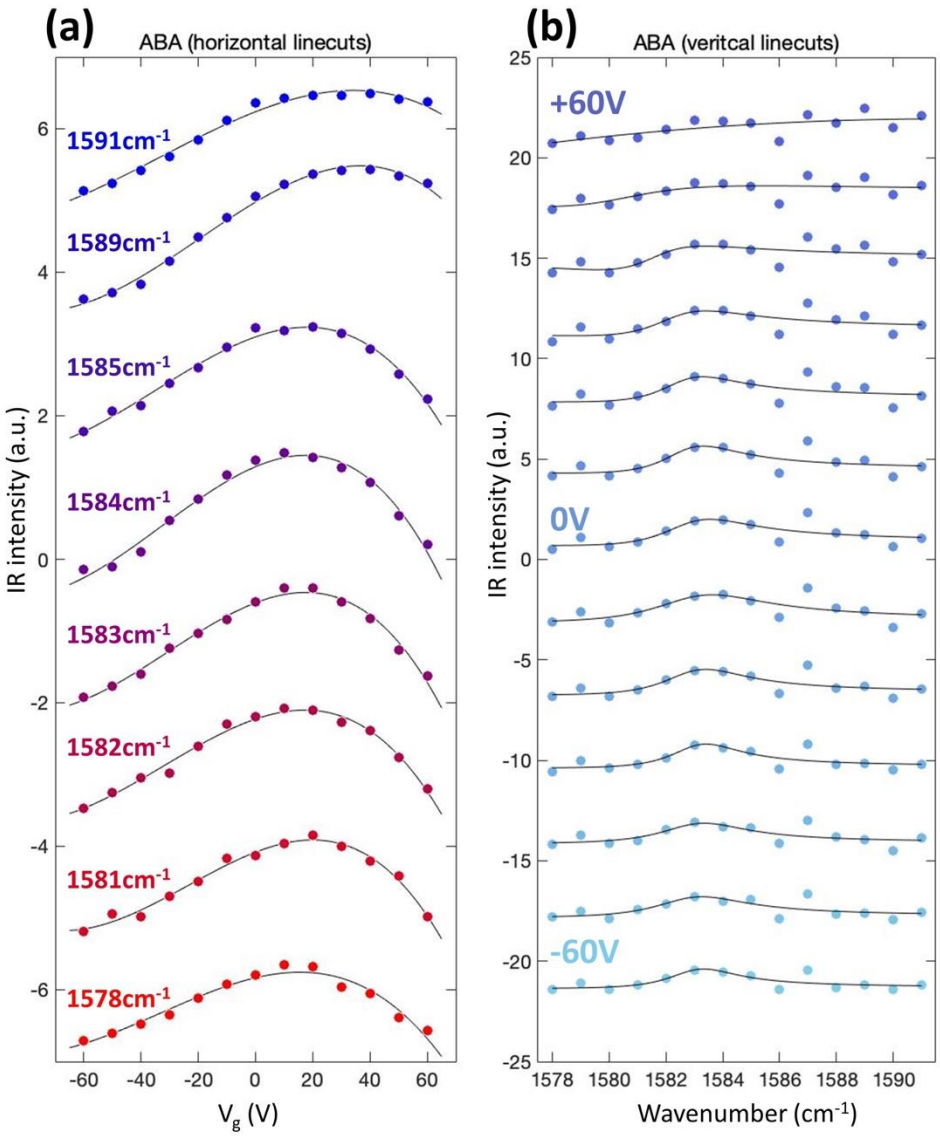

Figure S6. ABA trilayer's behaviors against both voltage and frequency. (a) Horizontal linecuts of Fig. 4a for ABA, showing the ABA trilayer's gate voltage dependence under different excitation frequencies. **(b)** Vertical linecuts of Fig. 4a for ABA, displaying the ABA trilayer's frequency dependence under different voltages. Compared to the ABC trilayer, the ABA trilayer behaves much more silently against the ingredients of both electric bias and excitation frequency.

Section V. The comparisons between Raman spectroscopy and SNOM.

In Fig. S7 we compare the SNOM method with the traditional Raman spectra for finding ABC domains. Beyond the resonance frequency, as Fig. S7a (1595 cm^{-1}), the region in the center of the pictures is darker. When the excitation is within the resonance region, as Fig. S7b (1585 cm^{-1}), the same region becomes bright, meaning that

this region is ABC-stacked. This result is in accordance with that judged by Raman (the bright yellow region in c), while the SNOM method has a much higher resolution which is only constrained by the AFM tip radius (~20 nm).

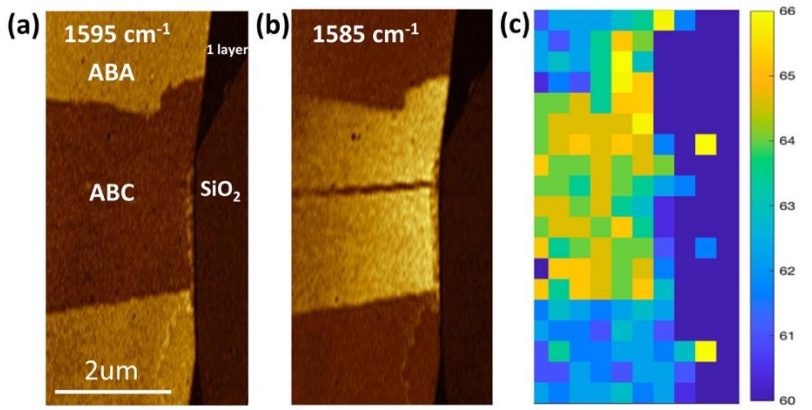

Figure S7. The contrast between Raman mapping and the SNOM images. (a-b) The near-field images for a trilayer sample with excitation at 1595 cm^{-1} and 1585 cm^{-1}, respectively. The contrast between ABC and ABA reverses when laser frequency is beyond (a) and within (b) the Fano resonance region. **(c)** The Raman mapping for half-width of the 2D peak in the same region. The bright region (yellow) has wider half width of 2D Raman peak, the feature for the ABC domain. The ABC domains distinguished by the SNOM method are in agreement with that judged by the traditional Raman mappings with much higher resolution.

Section VI. ABC trilayer's Fano resonance via initial doping.

It is a common phenomenon that samples that are primarily doped. As the two typical samples exhibited in Fig. S8a-d, the ABC domains turn bright when excitation is near the phonon frequency even without external bias applied, the merit of initial doping. In general, the samples with initial doping are in the majority. This enables the possibility to distinguish ABC graphene without the trouble to make a metal gate first. But note that it is not applied to all the samples. As e-g shows, some samples are near their charge-neutral states initially, and for these samples, the resonance phenomena of ABC can only be observed with a high gate applied.

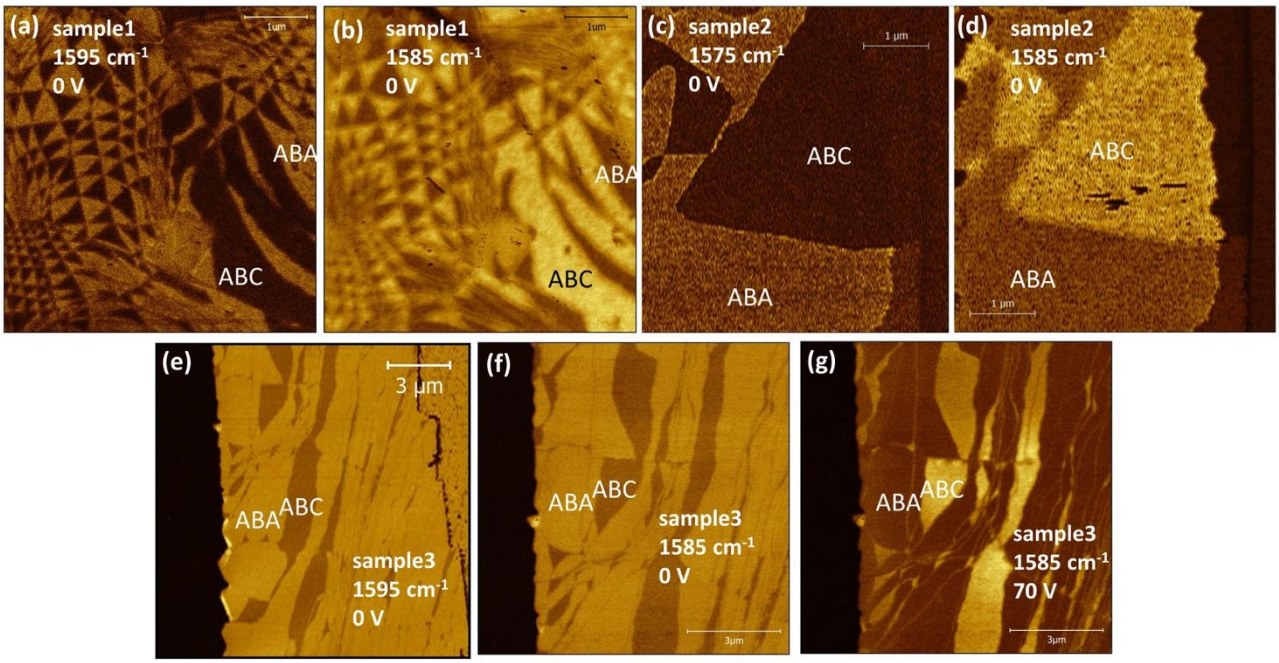

Figure S8. ABC's Fano resonance with initial doping. (a-b) are for the same sample without a gate applied and with frequency at 1595 cm^{-1} and 1585 cm^{-1}, respectively. Significant changes between ABA and ABC happen in this sample at its initial state due to this high intrinsic doping. **(c-d)** show another sample with similar phenomena as (a-b). **(e-g)** show another typical sample, in which the ABC didn't turn brighter than ABA when frequency changed from 1595 cm^{-1} (e) to 1585 cm^{-1} (f) without a gate applied, because its intrinsic state is closer to the charge neutral point. For this case, only when the gate voltage is set at a high value, like (g) in 1585 cm^{-1} and V_g=+70V, the ABC has a strong response.

Reference:

1. Hao, Y. F.; Wang, Y. Y.; Wang, L.; Ni, Z. H.; Wang, Z. Q.; Wang, R.; Koo, C. K.; Shen, Z. X.; Thong, J. T. L., Probing Layer Number and Stacking Order of Few-Layer Graphene by Raman Spectroscopy. *Small* **2010,** *6* (2), 195-200.

2. Lui, C. H.; Li, Z. Q.; Chen, Z. Y.; Klimov, P. V.; Brus, L. E.; Heinz, T. F., Imaging Stacking Order in Few-Layer Graphene. *Nano Lett* **2011,** *11* (1), 164-169.

3. - Effects of Configuration Interaction on Intensities and Phase Shifts. **1961,** - *124* (- 6), - 1878.

4. Lui, C. H.; Cappelluti, E.; Li, Z. Q.; Heinz, T. F., Tunable Infrared Phonon Anomalies in Trilayer Graphene. *Phys Rev Lett* **2013,** *110* (18).

5. Cong, C. X.; Yu, T.; Sato, K.; Shang, J. Z.; Saito, R.; Dresselhaus, G. F.; Dresselhaus, M. S., Raman Characterization of ABA- and ABC-Stacked Trilayer Graphene. *Acs Nano* **2011,** *5* (11), 8760-8768.